THE JOURNAL OF PHYSICAL CHEMISTRY C
A JOURNAL OF THE AMERICAN CHEMICAL SOCIETY

pubs.acs.org/JPCC Article

Probing into the Catalytic Activity of Single-Atom Catalysts for NO Oxidation by H_2O_2 via the Tri-activity Volcano Plot

Weijie Yang,* Xiang Li, Ruiyang Shi, Mingye Huang, Liugang Chen, Yixiao Sun, Yanfeng Liu, and Zhengyang Gao*

Cite This: J. Phys. Chem. C 2024, 128, 20569−20578 Read Online

ACCESS | Metrics & More | Article Recommendations | Supporting Information

ABSTRACT: The recently emerging single-atom catalysts (SACs) are proposed as promising candidates for the catalytic oxidation of NO in the field of NO pollutant reduction from coal-fired power stations. However, due to the lack of theoretical model guidance, achieving efficient catalytic oxidation of NO at room temperature still remains a major concern. Thus, in this study, the reaction pathways for the catalytic oxidation of NO by OOH radicals on eight TM−N_4−C (TM = Sc, Cr, Mn, Fe, Co, Ni, Cu, and Zn) were investigated based on density functional theory calculations. Based on the Bronsted−Evans−Polanyi linear relationship and microkinetic simulations, the activity volcano plot model for the catalytic oxidation of NO by OOH has been successfully established and validated. The Fe−N_4−C and Mn−N_4−C catalysts showed higher reactivities among these catalysts. The energy barriers for the rate-determining steps of these two catalysts were 0.14 and 0.30 eV, respectively, illustrating that catalytic oxidation of NO is feasible at room temperature. Significantly, a tri-activity volcano plot was constructed based on the unified activity descriptor of O adsorption energy for guiding the design of SACs in H_2O_2 catalytic oxidation of NO. The pathway of catalytic oxidation NO by OOH radicals is the dominant route in the system of SACs for the catalytic oxidation of NO by H_2O_2. The analysis of Bader charge and electronegativity revealed a linear correlation between the structural properties of the catalysts and the catalytic activity descriptor, which can be used to quickly predict the reactivity of SACs with different coordination environments. This work provides a new pathway for the current NO oxidation and guides future work on catalyst screening and experimental preparation.

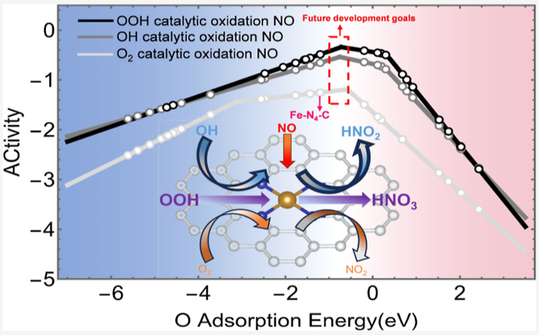

1. INTRODUCTION

The nitrogen oxide generated by coal combustion in power plants accounts for a large proportion of NO, and the NO emitted into the air poses great challenges to environmental governance and human health.[1,2] Catalytic oxidation technology is an effective means of removing NO, which can oxidize NO molecules into high-valence low-toxicity substances and apply them in industry.[3,4] However, most of the catalysts currently available for NO oxidation require high reaction rates at higher temperatures, which undoubtedly leads to resource consumption and restricts the development of NO catalytic oxidation technology.[5] In the current dual carbon economic environment, developing low-temperature and high-efficiency NO catalytic oxidation technology has become an urgent task. Thus, studying and identifying catalysts with high NO oxidation activity under low-temperature conditions are necessary.

Recent years have seen a significant focus on carbon-based single-atom catalysts (SACs) due to their strong catalytic activity and selectivity in various applications such as electrochemical catalytic reduction, hydrogen storage materials, and pollutant treatment.[6−9] Research on the catalytic oxidation of NO with O_2 and other oxidants indicates the effective performance of SACs. For example, Gao et al.[10] utilized density functional theory (DFT) calculations to investigate the possible oxidation mechanisms of NO and O_2 on the (Fe, Co)/N-GN catalyst in terms of kinetics and thermodynamics. The results indicate that O_2 can easily oxidize NO to NO_2; however, the energy barrier for subsequent product desorption is as high as 1.45 eV. Yang et al.'s[11] study found that the Fe/SV catalyst demonstrates high catalytic performance for NO oxidation, with the reaction mechanism revealed through DFT calculations. It was observed that the Eley−Rideal (E−R) mechanism predominantly governs NO oxidation, featuring a very low activation energy. While the reaction rate increases with increasing temperature, the equilibrium is inhibited. Wang and Guo[12] reported a series of activation potentials supporting the oxidation and reduction of NO by three-dimensional (3D)

Received: September 11, 2024
Revised: October 31, 2024
Accepted: November 13, 2024
Published: November 21, 2024

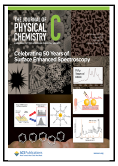

ACS Publications

https://doi.org/10.1021/acs.jpcc.4c06149

transition metal (TM) atoms on N-coordinated tuned graphene (GR). The research reveals that the N coordination pattern greatly affects the catalytic reactivity. Notably, Ti−N_3−GR stands out as the most promising candidate, demonstrating exceptional chemical activity and facilitating the reduction of NO to N_2 at ambient temperature. The oxidation study of NO was also carried out using O_2 as an oxidant with a reaction-determining step energy barrier of 1.12 eV. The above results indicate that SACs have demonstrated unique performance in the field of NO catalytic oxidation, but most oxidants require a high temperature to achieve high conversion rates, which leads to significant energy consumption. Therefore, the urgent task is to improve nitrogen oxide removal technology by finding a highly active oxidant that can take place at room temperature.

Advanced oxidation methods have attracted a lot of researchers' interest in recent years due to their high oxidation activity and fast reaction rates.[13−16] The research on the activation of H_2O_2 to generate OOH radicals for catalytic oxidation of pollutants is highly favored and has been widely applied. For example, Xu et al.[17] confirmed the formation of the key species *OOH in heterogeneous systems by enhanced Raman spectroscopy (SHINERS), isotopic labeling, and theoretical calculations on nanoparticles isolated from in situ shell layers. Compared with *H_2O_2, *OOH is more conducive to the charge transfer behavior and the activation of the O−O bond with the catalyst. Meng et al.[18] used a low-priced TiO_2 catalyst for efficient NO_x oxidation in the low concentration O_3 and H_2O_2 system. It was found that H_2O_2 could be more easily activated to generate OOH radicals for NO catalytic oxidation after the introduction of O_3 molecules. Qian et al.[19] investigated a novel high-gravity advanced oxidation process that employs an alkaline H_2O_2 solution as a liquid oxidizing agent. Under optimal conditions at ambient temperature, the process can achieve NO removal efficiencies of up to 99%. This improved efficiency in the HiGee-AOP/alkaline H_2O_2 process is due to the strong attraction between the hydroperoxyl radical (−OOH) and NO. The improved NO removal efficiency of the HiGee-AOP/alkaline H_2O_2 process stems from the strong affinity of OOH for NO. From the above analysis, it is clear that H_2O_2 as well as OOH radicals have been extensively studied for pollutant treatment. However, few researchers have yet applied them to NO oxidation studies. Therefore, in this work, SACs combined with OOH radicals were used for the catalytic oxidation of NO in the expectation that a new pathway for NO removal could be found.

In this work, we investigated the reaction pathways for the catalytic oxidation of NO over eight TM−N_4−C catalysts based on DFT calculations using OOH radicals as oxidants. The linear relationship between the adsorption energy of the OOH radicals and the reaction and desorption energy barriers was established, and the reactivity volcano plot model for the catalytic OOH oxidation of NO was constructed with adsorption energy of the OOH as the descriptor. And a tri-activity volcano plot for the catalytic oxidation of NO was constructed with O adsorption energy as the unifying descriptor, and the reactivities of OOH and OH for the oxidation of NO were higher than that of O_2. Based on this, the catalytic activities of 21 carbon-based SACs with different active centers were rapidly predicted, and the highest reactivities were found for the SACs with Fe−N_4−C and Mn−N_4−C catalysts at the 3d, 4d, and 5d active-metal-centered ligands. It was found that Fe−N_4−C and Mn−N_4−C catalysts had the highest reactivity for SACs with 3d and 4d and 5d active metal centers, and the decisive step barriers for these two catalysts were 0.14 and 0.30 eV, respectively. Based on the electronic characterization, both charge transfer and electronegativity X are linearly related to the catalytic activity, and a rapid prediction of the catalytic activity for NO oxidation can be achieved from the electronic structure of the catalyst.

2. COMPUTATION AND MODELING METHODS

Vienna ab initio simulation program (VASP) was used for all DFT computations. The computer simulations were all performed using the projector augmented wave approach with a 450 eV energy cutoff.[20] Relevance interactions were computed using the generalized gradient approximation of the Perdew−Burke−Ernzerhof functional.[21] The adjustments of van der Waals interaction were taken into account by using the DFT-D3 framework.[22] The catalytic surface was simulated as a $(5 \times 3\sqrt{3})$ graphene unit cell, and a 20 Å vacuum layer was implemented to mitigate the periodic effects in the SACs model.[23] The *K*-points of 2 × 2 × 1 and 4 × 4 × 1 were used to sample the Brillouin zone for geometric optimization and the calculation of electronic characteristics. In this study, we investigated the reaction mechanism of NO oxidation using aqueous OOH on TM−N_4-C through spin-polarized DFT calculations with ISPIN set to 2 in the VASP INCAR file. When optimizing the structure, the convergence criterion of the interatomic force is 0.02 eV/Å. In the self-consistent calculation, the energy difference between each electronic step is considered to have reached the convergence criterion when it is 10^{-5} eV.[24] Figure S1 provides information from the energy and *k*-point experiments. In this paper, we considered both the accuracy and efficiency of the calculations, selecting appropriate energy cutoff and *K*-point settings as the theoretical calculation parameters based on the test results. The charges were analyzed using the analytical method of the Bader charge.[25]

In getting the transition state (TS) structure of the simulation process, the climbing image nudge elastic band[26,27] is employed to make a preliminary guess of the TS, followed by the improved dimer (IDM)[28] for accurate optimization of the previously obtained TS. The force convergence standard of the IDM method is 0.05 eV/Å. To verify the correctness of the TS, vibration frequency analysis was conducted with a displacement constraint of ±0.02 Å.[29] From the Supporting Information, the calculation formulas of the energy mentioned in this paper can be obtained.

3. RESULTS AND DISCUSSION

3.1. Catalyst Model.

Carbon vacancy engineering and nitrogen doping are simple modification methods used in the catalyst preparation process. Previous studies have shown that graphene-based catalysts doped with 4N coordination exhibit excellent catalytic performance.[30] Therefore, in this work, 3d TMs (Figure 1a) were selected as the active centers of graphene-based catalysts, with the central TM atom located at the center of the entire catalyst surface, surrounded by N and C atoms. There is only one reaction active site on the surface of the entire catalyst, and subsequent reaction processes occur at this site. The only determined reaction active site lays a prerequisite for the establishment of the reaction process. To establish the robustness of the catalyst model, the binding energies of the 8 catalysts used were validated (Figure 1b), showing that they are significantly higher than the cohesive

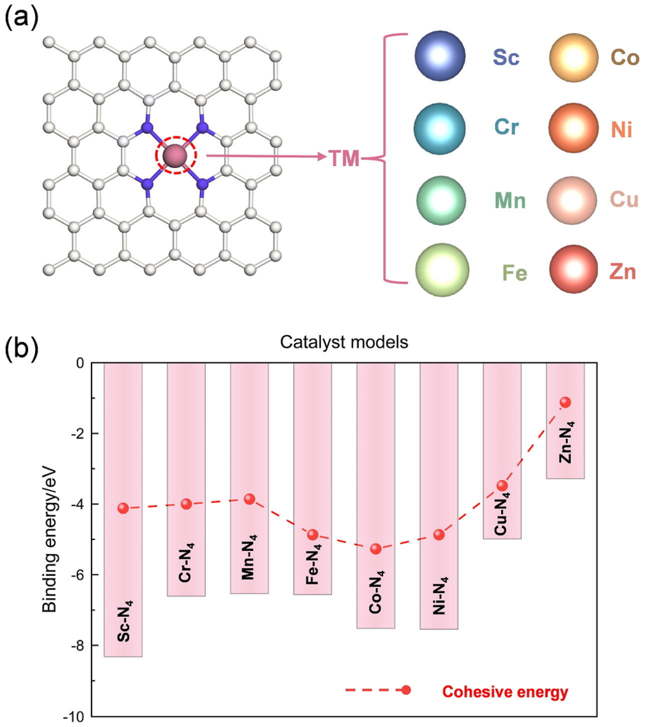

Figure 1. (a) Vertical views of the TM-N_4−C catalysts. The 3d single TM atoms (TM = Sc, Cr, Mn, Fe, Co, Ni, Cu, and Zn) were taken into consideration for this study. C, N, and TM atoms are represented by gray, blue, and pink, respectively. (b) Calculated binding energies and cohesive energies of 8 SACs.

energy values of the metal atoms,[31] thus confirming their suitability for subsequent NO catalytic oxidation research.

3.2. Reaction Mechanisms of NO Oxidation Using the OOH Radical.

The reaction pathway for H_2O_2 to generate OOH on TM-N_4−C has been well elucidated in our previous work.[33] Therefore, we focused on the oxidation process of NO by free radicals generated by H_2O_2. The oxidation state of nitrogen in the reactant NO is +2, which facilitates its conversion into high-value products such as NO_2, HNO_2, and HNO_3.[32] These products are harmless and can be resolved in the future. According to our previous investigations, HNO_3 emerges as the most likely product of NO oxidation catalyzed by OOH radicals on an Fe−N_4-C catalyst[33] due to it exhibiting the lowest energy barrier among the potential reaction pathways. The pathways for the catalytic reaction of NO by OOH radicals on SACs include the Langmuir−Hinshelwood[34] and E−R[35] reaction mechanisms. Our prior calculations indicate that the E−R mechanism functions concurrently across all SACs, leading us to identify it as the primary reaction pathway for oxidizing NO with OOH.

Previous studies have shown that there are two reaction pathways for the oxidation of NO catalyzed by OOH on SACs, and the final product of the OOH-catalyzed oxidation of NO is HNO_3. The HNO_3 molecule is a high-valence nitrate with extensive industrial applications; therefore, this reaction process has high economic value in industrial applications.[36,37] The most likely reaction pathway is the direct generation of HNO_3 from the oxidation of NO by the presence of OOH radicals. Therefore, in this section, this reaction process is adopted as the reaction mechanism on the TM−N_4−C catalyst for research.

3.3. Catalytic Oxidation of NO with the OOH Radical on SACs.

Figure 2a shows a schematic diagram of the catalytic oxidation of NO by OOH on the TM−N_4−C catalyst. The reaction process begins with the adsorption of OOH radicals onto the catalyst surface, forming an IM0 intermediate structure. Due to the difference in adsorption behavior between OOH radicals and NO molecules, there exists only an E−R reaction mechanism between the two. Then, NO molecules enter the vacuum layer on the upper side of the catalyst, forming the initial reaction structure IS1. As the reaction process progresses, the O−O bond of the OOH radical itself gradually breaks and NO molecules slowly interact with the catalyst surface. Finally, NO molecules are oxidized to form HNO_3 reaction products under the action of the OOH oxidant. After the product is generated, HNO_3 is desorbed from the catalyst surface and the SAC structure is restored to its initial state, completing the entire reaction process.

Using the Fe−N_4−C catalyst as an example, the specific reaction pathway for the OOH radical-catalyzed oxidation of NO is illustrated in Figure 2b. First, OOH radicals preferentially adsorb on the central active metal sites of SACs, becoming IM0 intermediates. Second, NO molecules enter the vacuum layer above the catalyst, forming the initial reaction state of IS1. Then, NO molecules gradually approach the catalyst surface and attack OOH molecules, causing O−O bonds to break and form TS configurations of O, OH, and NO. As shown in Figure 2b, we can see that when NO molecules attack the O_2 molecules, the O−O bond gradually lengthens from 1.48 Å of the initial configuration to 1.84 Å of the transition structure. As the reaction proceeds, HNO_3 products are ultimately generated. During the whole reaction process, the reaction energy barrier E_b is 0.14, and 1.06 eV of energy is released, which is thermodynamically favorable. The generated product HNO_3 will desorb from the catalyst surface and complete the entire reaction process. HNO_3 has no desorption energy barrier on Fe−N_4−C, and the product desorption process can be spontaneously completed. Meanwhile, Figures S2−S9 depict the reaction pathway associated with the catalytic oxidation of NO by OOH on various other SACs. Compared with the previous 1.33 eV[38,39] the rate-determining step energy barrier of NO oxidation by O_2 on SACs, the present study's exploration of NO oxidation catalyzed by OOH demonstrates extremely high reaction advantages.

To more intuitively analyze the energy changes of the OOH catalytic oxidation of NO on the TM−N_4−C catalyst, the sum of the energy of the OOH radicals, NO molecules, and catalyst structure is set as the zero-energy state. And proton conservation was applied to each intermediate state in the reaction process, making it possible to construct an energy ladder diagram that describes the reaction process. The energy profile diagram in Figure 2a, depicting the entire reaction process on 8 TM−N_4−C catalysts, enables us to classify all the catalysts into two distinct groups based on a comparison of their reaction energy barrier (E_b) and desorption energy barrier (E_d). First, the reaction energy barrier is higher than the desorption energy barrier, including Mn−N_4−C, Fe−N_4−C, Co−N_4−C, Ni−N_4−C, Cu−N_4−C, and Zn−N_4−C. Due to the unique oxidation performance of OOH radicals, NO can be oxidized to form HNO_3, a high-valence reaction product. HNO_3 is easily removed on weakly adsorbed SACs, making it a spontaneous reaction process. For such catalysts, the upper limit of activity throughout the entire reaction sequence is

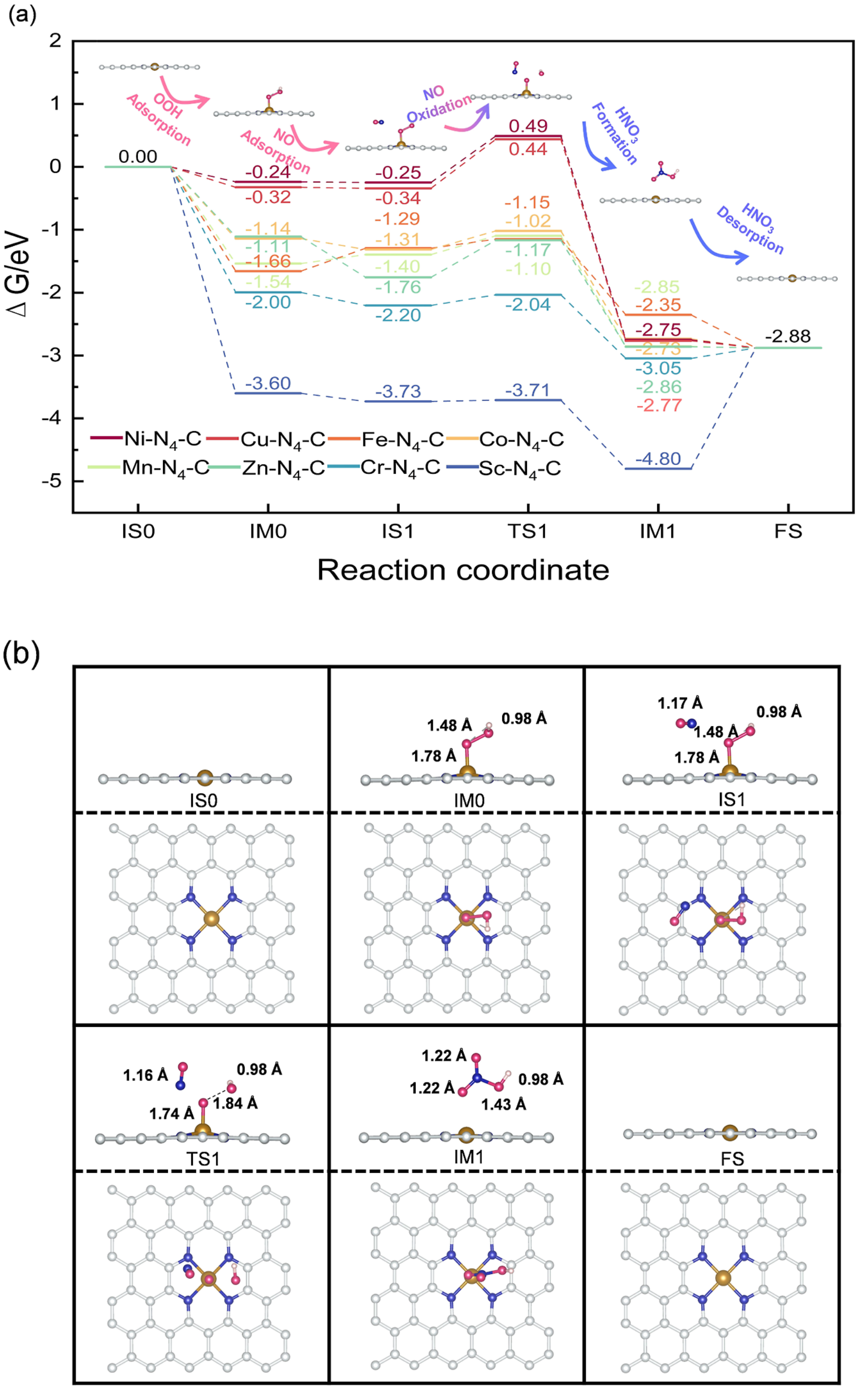

Figure 2. (a) Reaction cycle diagram of OOH catalytic oxidation of NO and energy variation diagram of the reaction process on 8 SACs. (b) Reaction pathway of catalytic oxidation of NO at Fe−N$_4$−C. C, N, O, and Fe are denoted by gray, blue, red, and brown, respectively.

contingent on the magnitude of the reaction energy barrier. The second type of catalysts, including Sc−N$_4$−C and Cr−N$_4$−C SACs, exhibit a lower reaction energy barrier than the desorption barrier, facilitating NO oxidation but hindering HNO$_3$ removal, thereby limiting the overall reaction process's activity upper limit due to their strong adsorption properties.

Given the analysis above, an enlightening observation is that catalysts with high reaction activity must have a moderate reaction energy barrier and desorption energy barrier.[40] By regulation of the central metal atoms and surrounding coordination atoms of the catalyst, the microelectronic properties of the catalyst can be controlled, thereby screening out catalyst structures with higher activity. The discovery of this pattern also provides a basis for the establishment of an activity volcano diagram model for catalytic oxidation of NO by OOH in the future.

3.4. Linear Relationship Analysis. The reaction kinetics of catalytic processes can be related to the fundamental thermodynamics underlying these processes.[41,42] Based on the micro reaction process and thermodynamic analysis explored above, a further analysis of the linear relationship between reaction kinetics and thermodynamics was conducted. This section mainly investigates the correlations between the adsorption energy of the OOH radicals on SACs and reaction

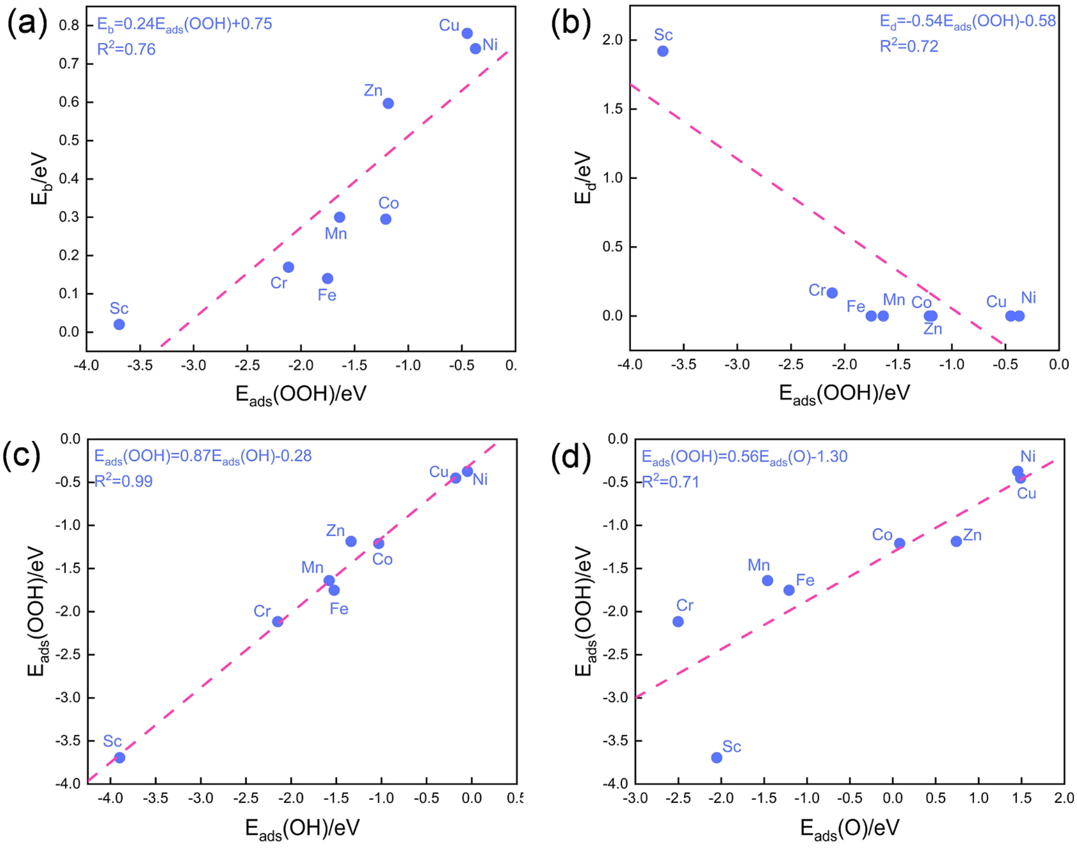

Figure 3. Correlation analyses of (a) E_b vs E_{ads} (OOH), (b) E_d vs E_{ads} (OOH), (c) E_{ads} (OH) vs E_{ads} (OOH), and (d) E_{ads} (O) vs E_{ads} (OOH).

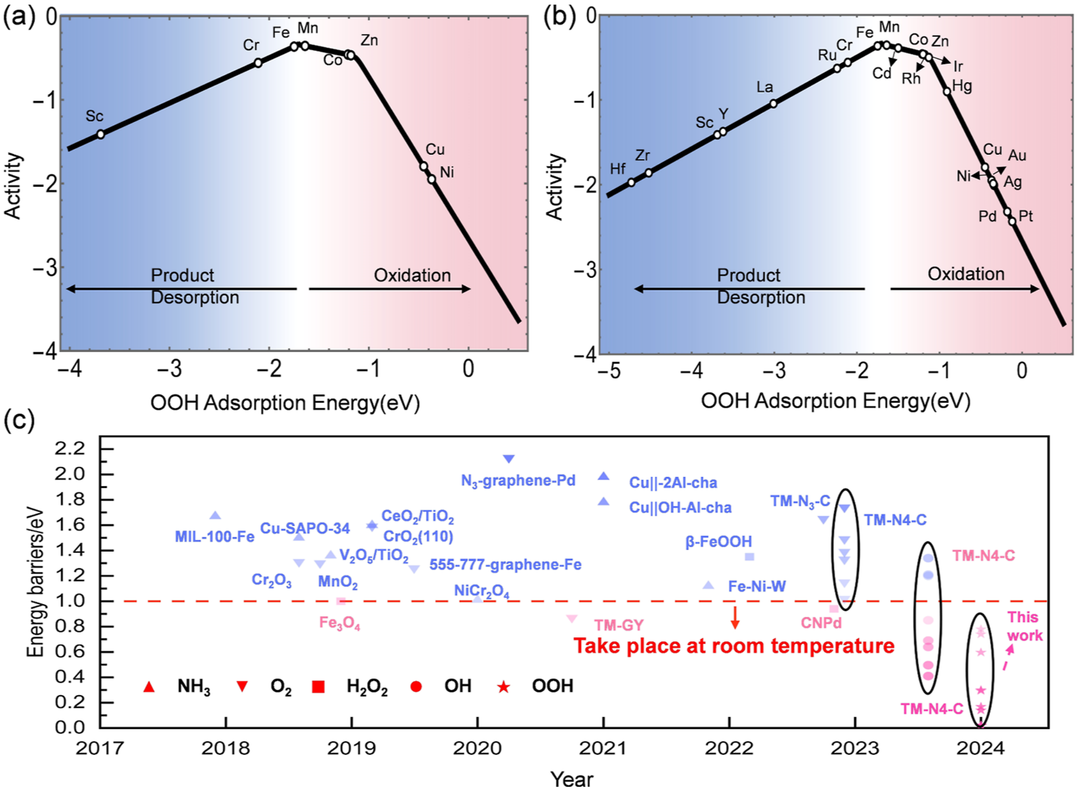

Figure 4. Volcano plots as a function of OOH adsorption energy with (a) 8 SACs explicitly analyzed in this study and (b) 21 TM−N_4−C SACs predicted in the study. (c) Scatter plot compared with previous studies of the NO reaction energy barrier.

energy barrier E_b and desorption energy barrier E_d. As shown in Figure 3a, the adsorption energy of the OOH radicals is linearly positively correlated with the reaction energy barrier E_b. As the adsorption energy of the OOH radicals decreases, the reaction energy barrier E_b of SACs toward NO increases. Figure 3b shows a significant negative relationship between the desorption energy barrier E_d and the OOH adsorption energy on a SAC, indicating that the desorption energy barrier E_d of a SAC decreases as the adsorption energy decreases. Given the linear relationship above, an enlightening rule can be found that changing the adsorption energy of a SAC toward OOH radicals will simultaneously affect its reaction energy barrier and desorption energy barrier, thereby affecting the overall activity of the catalyst structure. Therefore, to find catalysts with high reactivity, the adsorption strength of SACs for OOH radicals should be controlled within a reasonable range.

The activation products of H_2O_2 molecules mainly include active molecules, such as OH, O, and OOH radicals. In previous studies, the catalytic oxidation performance of OH radicals and O_2 molecules toward NO has been revealed.[39,43] This section mainly explores the oxidation performance of the OOH radicals on the NO molecules. After revealing the catalytic oxidation performance of OOH radicals on NO, the relationship between OOH radicals and OH radicals and O_2 radicals is analyzed at the microelectronic level, hoping to reveal their inherent connection. As shown in Figure 3c, a linear analysis was conducted on the adsorption energy of OOH radicals and OH radicals on SACs. Interestingly, a strong linear correlation exists between the two, with a linear correlation index R^2 close to 1. This indicates that the kinetic reaction characteristics and other properties of the OOH and OH adsorption energies can be compared under the same standard. Figure 3d shows the linear analysis between the adsorption energy of the OOH radicals and the adsorption energy of the O adsorption energy, and it is also found that there is a strong linear correlation between the two, indicating that the oxidation performance of the OOH radicals and the oxidation performance of the O_2 molecules toward NO can also be screened at the same level.

3.5. Microkinetic Analysis. Building on the analysis above, a distinct linear relationship exists among the adsorption energy of OOH, E_b and E_d in the catalytic oxidation of NO by OOH radicals. Therefore, considering OOH adsorption energy as a descriptor and analyzing the intrinsic relationship between thermodynamics and kinetics, the theoretical activity of different catalysts can be successfully predicted. To be consistent with the actual operating conditions, the same simulation conditions as previous studies[33,43] were used to conduct micro kinetic simulations of OOH catalytic oxidation of NO. Figure 4a demonstrates the establishment of a one-dimensional volcano plot model, utilizing the adsorption energy of OOH radicals as a descriptor. Eight SACs were plotted on the graph, and it can be seen that the upper limit of reaction activity of the catalysts on the left and right sides of the volcano plot vertex is determined by the HNO_3 desorption energy barrier and energy barrier of the reaction process, respectively. Among all SACs, Mn−N$_4$−C and Fe−N$_4$-C catalysts are the closest to the vertex of the volcano plot, and the corresponding adsorption energy value of the OOH free radical at the vertex of the volcano plot is −1.75 eV.

On this basis, to expand the prediction range, the OOH adsorption energy on SACs with active central metal elements from the 4d and 5d periods was also calculated, resulting in theoretical predicted values for their rates (Figure 4b). It is evident that Mn−N$_4$−C and Fe−N$_4$−C continue to outperform the other 21 SACs, further indicating that Mn−N$_4$−C and Fe−N$_4$−C catalysts exhibit efficient catalytic oxidation activity toward NO. At the same time, it can be found from Figure 4c that the energy barrier value in the catalytic oxidation of NO studied by predecessors is relatively high, which requires a higher temperature for the reaction to occur. But the OOH racial we employed in this work shows a lower energy barrier, indicating that this reaction can take place at room temperature.

The catalytic oxidation characteristics of NO by OH and O_2 have been studied in previous studies.[39,43] Combined with the exploration of the OOH catalytic oxidation of NO, the overall activity of H_2O_2 catalytic oxidation of NO on SACs has been revealed, including the catalytic oxidation of NO by O_2, OH, and OOH, respectively. Because previous studies have found a linear relationship between the adsorption energy of OH, OOH, and O over SACs, the adsorption energy of O can be a descriptor to simultaneously fit the activity volcano plot of OH and OOH catalyzing the oxidation of NO (Figure 5). It is clear that the activity trends of these three volcano plots are identical, and there is an activity vertex in each of them. Among all predicted SACs, the Fe−N$_4$−C catalyst showed the highest reaction activity. For the reaction pathway of NO oxidation using OOH, OH, and O_2, their rate-determined step energy barriers are those of the product desorption process. For the OOH catalytic oxidation of NO, the energy barrier for HNO_3 desorption is 0.53 eV. And the energy barriers for the desorption process of the NO product from the catalytic oxidation of NO by OH and O_2, which is the rate-determining step, are 0.86 and 1.33 eV, respectively. It can also be visually observed that the catalytic activity of OOH and OH for the oxidation of NO is significantly better than that of O_2, and the advanced oxidizing ability of H_2O_2 for the catalytic oxidation of NO has been verified, providing theoretical support for the subsequent development of the field of NO oxidation.

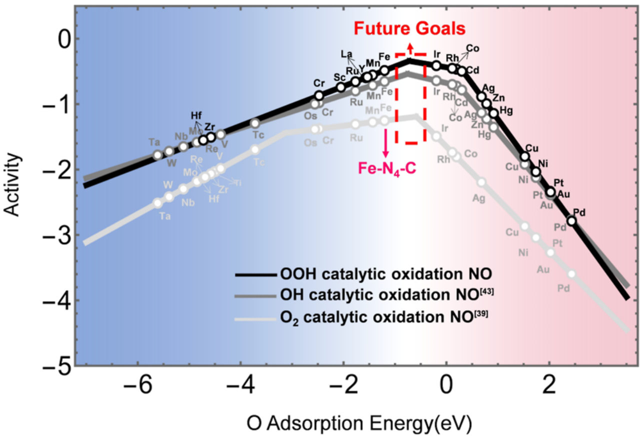

Figure 5. Tri-activity volcano plot of H_2O_2 catalytic oxidation of NO based on O adsorption energy.

Compared with traditional oxidants,[44,45] the study of OOH and H_2O_2 in NO catalytic oxidation in this article has a smaller reaction energy barrier and high reaction activity. Based on the study of the tri-activity volcano plot of H_2O_2 catalytic oxidation of NO in this article, it is hoped to provide new ideas for

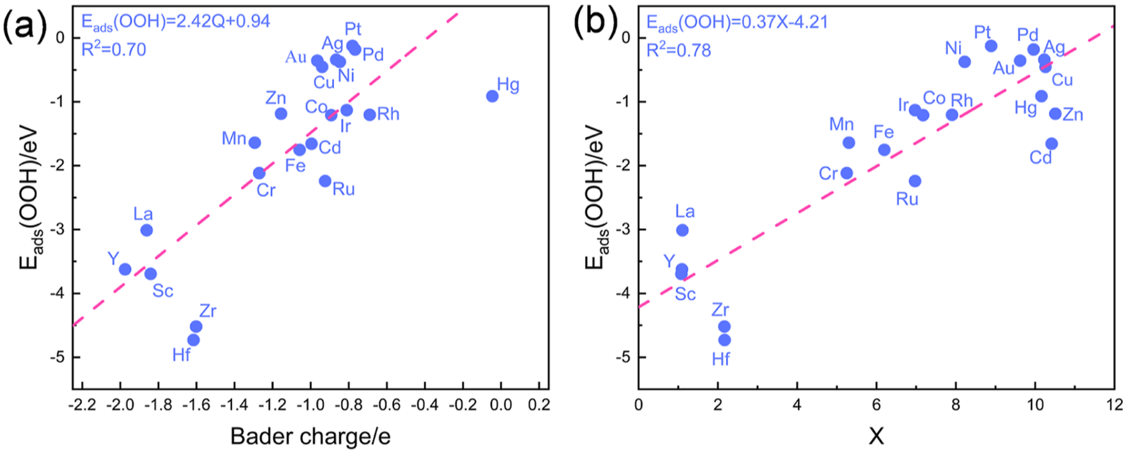

Figure 6. Linear correlations of (a) E_{ads} (OOH) vs Bader charge. (b) E_{ads} (OOH) vs electronegativity (X).

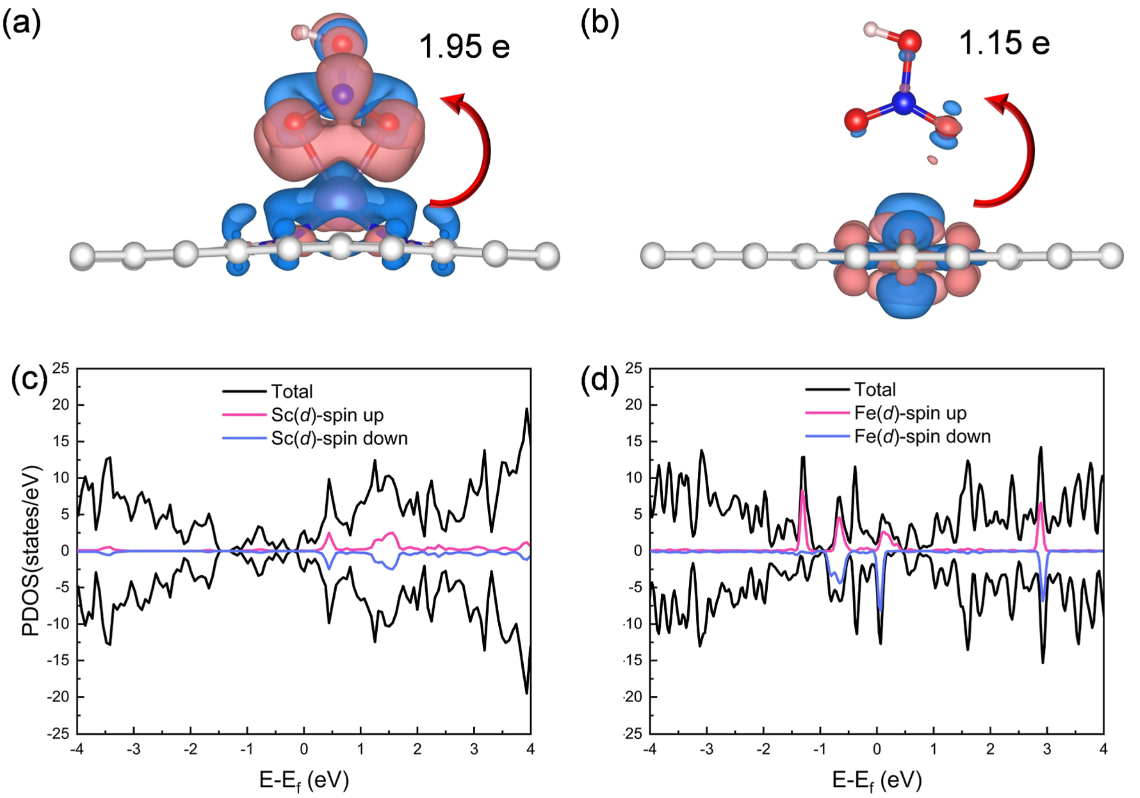

Figure 7. EDD between different SACs and HNO_3: (a) Sc−N_4−C and (b) Fe−N_4−C. PDOS analysis of different SACs: (c) Sc−N_4−C and (d) Fe−N_4−C. Red and blue areas represent electron gain and loss, respectively.

subsequent NO catalytic oxidation and effectively promote the further development of NO oxidation.

3.6. Electronic Characteristics. The catalytic activity of SACs is significantly influenced by their electronic properties, which occupy a pivotal position in determining their effectiveness.[46,47] In this section, the microelectronic properties of different catalysts were calculated to better predict and guide the adsorption energy intensity of the OOH radical across various SACs, including the Bader charge and electronegativity X of 21 SACs. And it is observed that a clear linear relationship exists between Bader charge and OOH radical adsorption energy, indicating a correlation between Bader charge transfer in SACs and OOH adsorption strength (Figure 6a). In addition, it was also found that there exists a significant linear relationship between the electronegativity X of 21 SACs and the adsorption energy of OOH radicals (Figure 6b). After analyzing the correlation between the different microelectronic properties and OOH adsorption energy of the OOH radicals on SACs, the corresponding adsorption energy of the OOH radicals can be obtained by simply calculating the electronic properties of different catalysts, and then, their performance for NO catalytic oxidation can be obtained through the above micro kinetic relationship.

At the same time, to reveal the inherent differences in the desorption energy barriers of different catalysts for HNO_3, electronic density difference (EDD) method[48] was used to analyze the bonding strength of the SAC structure and product

HNO_3 molecules. Through the charge density differential analysis in Figure 7a,b, it can be found that the red region is used to obtain electrons, while the blue region provides electrons. For a SAC structure, the active center is mostly surrounded by a blue region, indicating that the metal atom functions to supply electrons. The red area above the catalyst mainly surrounds the HNO_3 molecule, indicating that most electron transfer flows from the central metal atom to the HNO_3 molecule. For the Sc−N_4−C catalyst structure with strong adsorption, its adsorption effect on HNO_3 molecules is strong, and the energy barrier for the desorption process is relatively large; for catalyst structures with weaker adsorption such as Fe−N_4−C, the electron transfer between them and HNO_3 is relatively small, leading to a relatively weak bond strength between the active center and HNO_3, which often requires a smaller energy barrier during the product desorption process. The above analysis analyzed the cause of the differences in bonding strength between various SACs and HNO_3 at the microelectronic level and provided guidance for reducing the adsorption strength of catalysts on products in the future. The EDD analysis between other catalysts and HNO_3 is shown in Figure S10.

This section also investigates the projected density states (PDOS)[49] of eight 3d TM SACs, as shown in Figures 7c,d and S11. This analysis can demonstrate the degree of hybridization between atoms and reveal the changes in the electronic structure of the catalysts. Compared with some well-known magnetic elements with symmetric spin up and down PDOS (such as Fe, Co, and Ni), most metal elements exhibit relatively asymmetric PDOS in this TM−N_4−C coordination environment.[50] This indicates that there is a significant change in the spin state of TMs in this environment, leading to a significant change in catalytic performance compared to that of the bulk structure. The PDOS analysis of other catalysts is shown in Figure S11.

4. CONCLUSIONS

In conclusion, our study systematically investigated the reaction mechanism of catalytic oxidation of NO by OOH over SACs and developed an active volcano plot to predict catalyst performance. First, the reaction process of the OOH catalytic oxidation of NO over different SACs was explored based on DFT calculations to obtain the reaction energy barriers and energy changes. We identified a linear relationship between the adsorption energy of OOH radicals and both the reaction energy barriers E_b and the desorption energy barriers E_d, leading to the construction of a Bronsted−Evans−Polanyi model. Based on the classical Sabatier principle, a volcano plot model for OOH catalytic oxidation of NO on SACs was developed and successfully predicted for the 21 SACs we studied. And Fe−N_4−C and Mn−N_4−C catalysts exhibited the highest reactivity in 3, 4, and 5d SACs, which corresponded to decisive step energy barriers of 0.14 and 0.30 eV, respectively. These results indicate that OOH can catalyze the oxidation of NO at room temperature on the two SACs. Second, a strong linear correlation between adsorption energies of the OOH and those of both O and OH was found, and a 3D model for the oxidation of NO by H_2O_2 was established with the adsorption energies of the O adsorption atoms as the unified descriptor. The tri-activity volcano plots provide an overall comparison of the three reaction pathways, and it is found that the Fe−N_4−C catalyst exhibits the best oxidizing activity and receives an accurate descriptor to guide the subsequent catalyst screening. Moreover, our findings indicated that the catalytic oxidation of NO by OH and OOH exhibits significantly higher reactivity than that by O_2, highlighting the high efficacy of OOH and OH in NO oxidation processes. Finally, charge transfer and electronegativity X were found to be linearly correlated with the adsorption strength of the OOH radicals at the same time by the microelectronic structure analysis, which can predict the period reaction activity by the catalyst electronic structure. This article reveals a novel reaction pathway for NO catalytic oxidation, providing a theoretical basis for subsequent catalyst screening and experimental preparation.

■ ASSOCIATED CONTENT

Supporting Information

The Supporting Information is available free of charge at https://pubs.acs.org/doi/10.1021/acs.jpcc.4c06149.

Calculated parameters for the structure of TM-N_4−C catalysts *k*-point and energy cutoff tests, reaction pathway of catalytic oxidation of NO at TM−N_4−C, EDD between different SACs and HNO_3, and PDOS analysis of different SACs (PDF)

■ AUTHOR INFORMATION

Corresponding Authors

Weijie Yang − *Department of Power Engineering, North China Electric Power University, Baoding, Hebei 071003, China; Hebei Key Laboratory of Low Carbon and High-Efficiency Power Generation Technology, North China Electric Power University, Baoding, Hebei 071003, China;* orcid.org/0000-0002-0232-1129; Email: yangwj@ncepu.edu.cn

Zhengyang Gao − *Department of Power Engineering, North China Electric Power University, Baoding, Hebei 071003, China; Hebei Key Laboratory of Low Carbon and High-Efficiency Power Generation Technology, North China Electric Power University, Baoding, Hebei 071003, China;* Email: gaozhyan@163.com

Authors

Xiang Li − *Department of Power Engineering, North China Electric Power University, Baoding, Hebei 071003, China; Hebei Key Laboratory of Low Carbon and High-Efficiency Power Generation Technology, North China Electric Power University, Baoding, Hebei 071003, China*

Ruiyang Shi − *Department of Power Engineering, North China Electric Power University, Baoding, Hebei 071003, China; Hebei Key Laboratory of Low Carbon and High-Efficiency Power Generation Technology, North China Electric Power University, Baoding, Hebei 071003, China*

Mingye Huang − *Department of Power Engineering, North China Electric Power University, Baoding, Hebei 071003, China; Hebei Key Laboratory of Low Carbon and High-Efficiency Power Generation Technology, North China Electric Power University, Baoding, Hebei 071003, China*

Liugang Chen − *Department of Power Engineering, North China Electric Power University, Baoding, Hebei 071003, China; Hebei Key Laboratory of Low Carbon and High-Efficiency Power Generation Technology, North China Electric Power University, Baoding, Hebei 071003, China*

Yixiao Sun − *Department of Power Engineering, North China Electric Power University, Baoding, Hebei 071003, China;*

Hebei Key Laboratory of Low Carbon and High-Efficiency Power Generation Technology, North China Electric Power University, Baoding, Hebei 071003, China

Yanfeng Liu − *Department of Power Engineering, North China Electric Power University, Baoding, Hebei 071003, China; Hebei Key Laboratory of Low Carbon and High-Efficiency Power Generation Technology, North China Electric Power University, Baoding, Hebei 071003, China*

Complete contact information is available at: https://pubs.acs.org/10.1021/acs.jpcc.4c06149

Notes

The authors declare no competing financial interest.

■ ACKNOWLEDGMENTS

This work was funded by the National Natural Science Foundation of China (nos. 52176104 and 52006073).

■ REFERENCES

(1) Dong, J.; Gao, Z.; Yang, W.; Li, A.; Ding, X. Adsorption characteristics of Co-anchored different graphene substrates toward O2 and NO molecules. *Appl. Surf. Sci.* **2019**, *480*, 779−791.

(2) Cao, F.; Su, S.; Xiang, J.; Wang, P.; Hu, S.; Sun, L.; Zhang, A. The activity and mechanism study of Fe−Mn−Ce/γ-Al2O3 catalyst for low temperature selective catalytic reduction of NO with NH3. *Fuel* **2015**, *139*, 232−239.

(3) Talib, S. H.; Hussain, S.; Baskaran, S.; Lu, Z.; Li, J. Chromium Single-Atom Catalyst with Graphyne Support: A Theoretical Study of NO Oxidation and Reduction. *ACS Catal.* **2020**, *10* (20), 11951−11961.

(4) Yang, W.; Liu, X.; Chen, X.; Cao, Y.; Cui, S.; Jiao, L.; Wu, C.; Chen, C.; Fu, D.; Gates, I. D.; et al. A Sulfur-Tolerant MOF-Based Single-Atom Fe Catalyst for Efficient Oxidation of NO and Hg0. *Adv. Mater.* **2022**, *34* (20), 2110123.

(5) Yang, W.; Huang, H.; Liu, X.; Ren, J.; Ma, K.; Pan, Z.; Ding, Z.; Ding, X.; Gao, Z. Screening the activity of single-atom catalysts for the catalytic oxidation of sulfur dioxide with a kinetic activity model. *Chem. Commun.* **2020**, *56* (78), 11657−11660.

(6) Yang, W.; Chen, X.; Feng, Y.; Wang, F.; Gao, Z.; Liu, Y.; Ding, X.; Li, H. Understanding trends in the mercury oxidation activity of single-atom catalysts. *Environ. Sci.: Nano* **2022**, *9* (6), 2041−2050.

(7) Zhang, Y.; Yang, R.; Li, H.; Zeng, Z. Boosting Electrocatalytic Reduction of CO2 to HCOOH on Ni Single Atom Anchored WTe2Monolayer. *Small* **2022**, *18* (44), 2203759.

(8) Li, H.; Yu, B.; Zhuang, Z.; Sun, W.; Jia, B.; Ma, T. A small change in the local atomic environment for a big improvement in single-atom catalysis. *J. Mater. Chem. A* **2021**, *9* (7), 4184−4192.

(9) Liu, J.; Zhang, G.; Ye, K.; Xu, K.; Sheng, Y.; Yu, C.; Zhang, H.; Li, Q.; Liang, Z.; Jiang, K. Top-down manufacturing of efficient CO2 reduction catalysts from the gasification residue carbon. *Chem. Commun.* **2023**, *59* (5), 611−614.

(10) Gao, Z.; Liu, X.; Li, A.; Li, X.; Ding, X.; Yang, W. Bimetallic sites supported on N-doped graphene ((Fe,Co)/N-GN) as a new catalyst for NO oxidation: A theoretical investigation. *Mol. Catal.* **2019**, *470*, 56−66.

(11) Yang, W.; Gao, Z.; Liu, X.; Li, X.; Ding, X.; Yan, W. Single-atom iron catalyst with single-vacancy graphene-based substrate as a novel catalyst for NO oxidation: a theoretical study. *Catal. Sci. Technol.* **2018**, *8* (16), 4159−4168.

(12) Wang, C.; Guo, C. Nitrogen atom coordination tuned transition metal catalysts for NO oxidation and reduction. *Chemosphere* **2022**, *309*, 136735.

(13) Hao, Y.; Li, Y.; Wu, J.; Meng, L.; Wang, J.; Jia, C.; Liu, T.; Yang, X.; Liu, Z.-P.; Gong, M. Recognition of Surface Oxygen Intermediates on NiFe Oxyhydroxide Oxygen-Evolving Catalysts by Homogeneous Oxidation Reactivity. *J. Am. Chem. Soc.* **2021**, *143* (3), 1493−1502.

(14) Cheng, Z.; Ling, L.; Wu, Z.; Fang, J.; Westerhoff, P.; Shang, C. Novel Visible Light-Driven Photocatalytic Chlorine Activation Process for Carbamazepine Degradation in Drinking Water. *Environ. Sci. Technol.* **2020**, *54* (18), 11584−11593.

(15) Weng, C.; Chuang, Y.-H.; Davey, B.; Mitch, W. A. Reductive Electrochemical Activation of Hydrogen Peroxide as an Advanced Oxidation Process for Treatment of Reverse Osmosis Permeate during Potable Reuse. *Environ. Sci. Technol.* **2020**, *54* (19), 12593−12601.

(16) Sharma, S.; Dutta, V.; Raizada, P.; Hosseini-Bandegharaei, A.; Singh, P.; Nguyen, V.-H. Tailoring cadmium sulfide-based photocatalytic nanomaterials for water decontamination: a review. *Environ. Chem. Lett.* **2021**, *19* (1), 271−306.

(17) Xu, X.; Zhang, Y.; Chen, Y.; Liu, C.; Wang, W.; Wang, J.; Huang, H.; Feng, J.; Li, Z.; Zou, Z. Revealing *OOH key intermediates and regulating H2O2 photoactivation by surface relaxation of Fenton-like catalysts. *Proc. Natl. Acad. Sci. U.S.A.* **2022**, *119* (36), No. e2205562119.

(18) Meng, F.; Guo, L.; Zou, H.; Zhu, B.; Zhou, F.; Zeng, Y.; Han, J.; Yang, J.; Zhang, S.; Zhong, Q. Mechanism study on TiO2 inducing O2- and OH radicals in O3/H2O2 system for high-efficiency NO oxidation. *J. Hazard. Mater.* **2020**, *399*, 123033.

(19) Qian, Z.; Zhang, J.; Wang, C.; Chen, H.; Zheng, J. A novel High-Gravity AOP process for enhanced NOx attenuation using alkaline H2O2 as a strong oxidizing reagent: Reaction mechanisms and kinetics. *Chem. Eng. J.* **2021**, *404*, 126454.

(20) Perdew, J. P.; Burke, K.; Ernzerhof, M. Generalized Gradient Approximation Made Simple. *Phys. Rev. Lett.* **1996**, *77* (18), 3865−3868.

(21) Kresse, G.; Joubert, D. From ultrasoft pseudopotentials to the projector augmented-wave method. *Phys. Rev. B: Condens. Matter Mater. Phys.* **1999**, *59* (3), 1758−1775.

(22) Grimme, S.; Antony, J.; Ehrlich, S.; Krieg, H. A consistent and accurate ab initio parametrization of density functional dispersion correction (DFT-D) for the 94 elements H-Pu. *J. Chem. Phys.* **2010**, *132* (15), 154104.

(23) Ma, L.; Zhang, J.-M.; Xu, K.-W.; Ji, V. A first-principles study on gas sensing properties of graphene and Pd-doped graphene. *Appl. Surf. Sci.* **2015**, *343*, 121−127.

(24) van Bree, R.; Gerrits, N.; Kroes, G.-J. Dissociative chemisorption of O2 on Al(111): Dynamics on a potential energy surface computed with a non-self-consistent screened hybrid density functional approach. *Faraday Discuss.* **2024**, *251*, 361−381.

(25) Henkelman, G.; Arnaldsson, A.; Jónsson, H. A fast and robust algorithm for Bader decomposition of charge density. *Comput. Mater. Sci.* **2006**, *36* (3), 354−360.

(26) Henkelman, G.; Jónsson, H. Improved tangent estimate in the nudged elastic band method for finding minimum energy paths and saddle points. *J. Chem. Phys.* **2000**, *113* (22), 9978−9985.

(27) Henkelman, G.; Uberuaga, B. P.; Jónsson, H. A climbing image nudged elastic band method for finding saddle points and minimum energy paths. *J. Chem. Phys.* **2000**, *113* (22), 9901−9904.

(28) Heyden, A.; Bell, A. T.; Keil, F. J. Efficient methods for finding transition states in chemical reactions: Comparison of improved dimer method and partitioned rational function optimization method. *J. Chem. Phys.* **2005**, *123* (22), 224101.

(29) Riplinger, C.; Carter, E. A. Cooperative Effects in Water Binding to Cuprous Oxide Surfaces. *J. Phys. Chem. C* **2015**, *119* (17), 9311−9323.

(30) Zhao, L.; Zhang, Y.; Huang, L.-B.; Liu, X.-Z.; Zhang, Q.-H.; He, C.; Wu, Z.-Y.; Zhang, L.-J.; Wu, J.; Yang, W.; Gu, L.; et al. Cascade anchoring strategy for general mass production of high-loading single-atomic metal-nitrogen catalysts. *Nat. Commun.* **2019**, *10* (1), 1278.

(31) Liu, X.; Xu, M.; Wan, L.; Zhu, H.; Yao, K.; Linguerri, R.; Chambaud, G.; Han, Y.; Meng, C. Superior Catalytic Performance of Atomically Dispersed Palladium on Graphene in CO Oxidation. *ACS Catal.* **2020**, *10* (5), 3084−3093.

(32) Song, Z.; Wang, B.; Yu, J.; Ma, C.; Chen, T.; Yang, W.; Liu, S.; Sun, L. Effect of Ti doping on heterogeneous oxidation of NO over

Fe3O4 (111) surface by H2O2: A density functional study. *Chem. Eng. J.* **2018**, *354*, 517−524.

(33) Yang, W.; Chen, L.; Zhou, B.; Jia, Z.; Liu, X.; Liu, Y.; Li, H.; Gao, Z. NO Oxidation Using H2O2 at a Single-Atom Iron Catalyst. *J. Phys. Chem. C* **2023**, *127* (27), 13011−13020.

(34) Negreira, A. S.; Wilcox, J. DFT Study of Hg Oxidation across Vanadia-Titania SCR Catalyst under Flue Gas Conditions. *J. Phys. Chem. C* **2013**, *117* (4), 1761−1772.

(35) Ling, L.; Han, P.; Wang, B.; Zhang, R. Theoretical prediction of simultaneous removal efficiency of ZnO for H2S and Hg0 in coal gas. *Chem. Eng. J.* **2013**, *231*, 388−396.

(36) Tan, N.; Han, S.; Wei, K.; Ma, W. Determination of Silicon Content in Metallurgical-Grade Silicon Refined Slag using Two-Step Dissolution Chemical Analysis Method. *Silicon* **2024**, *16* (1), 123−132.

(37) Shi, S.; Ma, B.; Zhao, D.; Li, X.; Shao, S.; Wang, C.; Chen, Y. Thermal behavior of Al(NO3)3·9H2O and its application in preparing Al2O3 and regenerating HNO3. *Process Saf. Environ. Prot.* **2023**, *178*, 728−738.

(38) Dong, S.; Wang, J.; Li, C.; Liu, H.; Gao, Z.; Wu, C.; Yang, W. Simultaneous catalytic oxidation mechanism of NO and Hg0 over single-atom iron catalyst. *Appl. Surf. Sci.* **2023**, *609*, 155298.

(39) Yang, W.; Feng, Y.; Chen, X.; Wu, C.; Wang, F.; Gao, Z.; Liu, Y.; Ding, X.; Li, H. Understanding Trends in the NO Oxidation Activity of Single-Atom Catalysts. *J. Environ. Chem. Eng.* **2022**, *10* (6), 108744.

(40) Dichter, G. S.; Smoski, M. J.; Kampov-Polevoy, A. B.; Gallop, R.; Garbutt, J. C. Unipolar depression does not moderate responses to the Sweet Taste Test. *Depress. Anxiety* **2010**, *27* (9), 859−863.

(41) Bligaard, T.; Nørskov, J. K.; Dahl, S.; Matthiesen, J.; Christensen, C. H.; Sehested, J. The Brønsted−Evans−Polanyi relation and the volcano curve in heterogeneous catalysis. *J. Catal.* **2004**, *224* (1), 206−217.

(42) Gao, M.; Cheng, C.; Miao, Z.; Wan, K.; He, Q. Physicochemical properties, combustion kinetics and thermodynamics of oxidized lignite. *Energy* **2023**, *268*, 126657.

(43) Yang, W.; Chen, L.; Jia, Z.; Zhou, B.; Liu, Y.; Wu, C.; Gao, Z. Design of single-atom catalysts for NO oxidation using OH radicals. *J. Mater. Chem. A* **2023**, *11* (43), 23249−23259.

(44) Si, C.; Yang, M.; Li, B. Revealing the Tunable Effects of Single Metal Atoms Supported on Nitrogen-Doped Carbon Nanotubes during NO Oxidation from Microkinetic Simulation. *J. Phys. Chem. C* **2022**, *126* (43), 18275−18281.

(45) Yang, W.; Zhou, B.; Chen, L.; Shi, R.; Li, H.; Liu, X.; Gao, Z. Coordination engineering for single-atom catalysts in bifunctional oxidation NO and mercury. *Fuel* **2023**, *349*, 128751.

(46) Liu, B.; Guo, W.; Si, Q.; Jia, W.; Zheng, S.; Wang, H.; Zhao, Q.; Luo, H.; Jiang, J.; Ren, N. Atomically dispersed cobalt on carbon nitride for peroxymonosulfate activation: Switchable catalysis enabled by light irradiation. *Chem. Eng. J.* **2022**, *446*, 137277.

(47) Daelman, N.; Capdevila-Cortada, M.; López, N. Dynamic charge and oxidation state of Pt/CeO2 single-atom catalysts. *Nat. Mater.* **2019**, *18* (11), 1215−1221.

(48) Cremer, D.; Kraka, E. Chemical Bonds without Bonding Electron Density — Does the Difference Electron-Density Analysis Suffice for a Description of the Chemical Bond? *Angew Chem. Int. Ed. Engl.* **1984**, *23* (8), 627−628.

(49) Hone, J.; Llaguno, M. C.; Biercuk, M. J.; Johnson, A. T.; Batlogg, B.; Benes, Z.; Fischer, J. E. Thermal properties of carbon nanotubes and nanotube-based materials. *Appl. Phys. A: Mater. Sci. Process.* **2002**, *74* (3), 339−343.

(50) Piao, Y.; Jiang, Q.; Li, H.; Matsumoto, H.; Liang, J.; Liu, W.; Pham-Huu, C.; Liu, Y.; Wang, F. Identify Zr Promotion Effects in Atomic Scale for Co-Based Catalysts in Fischer−Tropsch Synthesis. *ACS Catal.* **2020**, *10* (14), 7894−7906.